Influence of Flexible Appendages on Dual-Spin Spacecraft Dynamics and Control

AUSTIN H. GALE*
Hughes Aircraft Company, El Segundo, Calif.

AND

PETER W. LIKINS†
University of California, Los Angeles, Calif.

The influence of flexible antennas and solar panels on the dynamic behavior and control system response of a two-body spacecraft, one part of which may spin, is investigated. Space vehicles are modeled with a rigid platform to which are attached a rigid rotor, a damped linear oscillator (simulating a "nutation damper"), and one or more flexible appendages. Flexibility is accommodated by use of modal deformation coordinates for the appendages in combination with discrete coordinates of the platform, rotor and damper. The presence of a damper on a nonrotating platform would in the absence of flexibility and active control maintain the rotor spin axis in coincidence with the angular momentum vector. A third despin control system is designed to maintain attitude control of the platform about the bearing axis. Attitude control jets provide angular momentum control on command. Linearized equations provide the basis for digital simulation and for stability determination by eigenvalue analysis, permitting the assessment of the influence of flexible appendages on vehicle behavior.

Nomenclature

b = nominal distance from system mass to damper mass center (see Fig. 1)
d = dashpot viscosity constant of damper
C_T = damping coefficient of proportional despin control system
E^1 = $[100]^T$
E^2 = $[010]^T$
E^3 = $[001]^T$
F = matrix in platform basis of external force applied to the vehicle
i = superscript denoting the ith sub-body ($i = 1,2 \ldots n$)
I = inertia matrix for total vehicle in nominal configuration for mass center, in vector basis $\mathbf{b}_1$, $\mathbf{b}_2$, $\mathbf{b}_3$
$\mathcal{J}$ = moment of inertia of rotor R about $\mathbf{b}_3$ axis
j = moment of inertia ratio defined in Eq. (21)
k = spring constant of damper
K_C = gain factor in transfer function of third-order despin control system
K_T = spring constant of proportional despin control system
m = damper mass
M = $6n \times 6n$ matrix null except for 3×3 mass and inertia matrices of the appendage sub-bodies along the diagonal (n is the number of sub-bodies)
$\mathfrak{M}$ = total vehicle mass
p = angular momentum ratio defined in Eq. (21)
q = coordinate matrix of flexible appendage
R = matrix in B basis of vector from O to Q (see Fig. 1)
r^i = matrix in B basis from Q to Q^i (See Fig. 1)

$$\tilde{R} = \begin{bmatrix} 0 & -R_3 & R_2 \\ R_3 & 0 & -R_1 \\ -R_2 & R_1 & 0 \end{bmatrix} \text{ and } \tilde{r}^i = \begin{bmatrix} 0 & -r_3^i & r_2^i \\ r_3^i & 0 & -r_1^i \\ -r_2^i & r_1^i & 0 \end{bmatrix}$$

$$\tilde{r} = \begin{bmatrix} \tilde{r}^1 & & & & 0 \\ & 0 & & & \\ & & \tilde{r}^2 & & \\ & & & 0 & \\ & & & & \ddots \\ & & & & \tilde{r}^n \\ 0 & & & & 0 \end{bmatrix} \text{ in terms of } 3 \times 3 \text{ submatrices}$$

t_n = time at despin control system error sampling n
T = external torque applied to the vehicle (e.g., by attitude control jets or the gravity field)
$u_\alpha{}^i$ = deflection of sub-body i along the α axis relative to its undeformed position
v = variable representing frequencies corresponding to eigenvalues of the simplified Gyrostat system
V = v normalized by the simplified appendage fixed base frequency
x = column matrix in numerous variables defined in Eq. (1)
α = subscript denoting motion in the direction of or rotation about axes $\alpha = 1,2,3$
$\beta_\alpha{}^i$ = rotation of sub-bodies i about α axis relative to its undeformed position
γ = peak despin pointing error
ϵ = error in θ_c
δ = diagonal $N \times N$ matrix of appendage modal damping ratios for N modes
δ_p, δ_z = damping ratios in the transfer function of the third-order despin control system
η = $N \times 1$ truncated matrix of appendage modal coordinates (N is the number of modes)
θ = $[\theta_1\theta_2\theta_3]^T$, where $\theta_1\theta_2\theta_3$ define inertial attitude of B
θ_c = desired stator pointing angle about axis 3
θ_p = stator pointing angle used between times of data sampling (equals θ_3 at sampling time.)
κ = spring constant in bending of the simplified appendage
λ = matrix of forces and torques applied to the sub-bodies of the appendage
μ = singular mass simulating the simplified appendage
ξ = displacement of damper mass in direction of $\mathbf{b}_1$ (see Fig. 1)
σ^2 = diagonal $N \times N$ matrix of the squares of natural frequencies of appendage vibration

Received January 5, 1970; revision received April 10, 1970. This study was supported by Hughes Aircraft Company, Space Systems Division.

* Senior Staff Engineer, Space Systems Division, Structural Mechanics Department. Member AIAA.

† Associate Professor of Engineering; also Consultant, Space Systems Division, Hughes Aircraft Company. Associate Fellow AIAA.

Σ_{EO} = $[EOEO \ldots EO]^T$, where E is the 3 × 3 identity matrix and O is the 3 × 3 null matrix
Σ_{OE} = $[OEOE \ldots OE]^T$
τ = magnitude of control torque applied to rotor about bearing axis (so $-\tau \mathbf{b}_3$ is applied to B)
φ = rotation of the rotor R relative to the platform, B
Φ = $6n \times$ N transformation matrix from discrete to modal appendage deformation coordinates (so in Eq. (5) $q = \Phi\eta$), normalized so that $\Phi^T M \Phi$ is an identity matrix
ω_p, ω_z = frequencies in the transfer function of the third-order despin control system
Ω = nominal angular rate of the rotor relative to B

Introduction

THE term "dual-spin" has been applied to any space vehicle which consists of two primary bodies capable of relative rotation about a common axis. Prominent early examples of satellites of this configuration are the OSO (Orbiting Solar Observatory) series, the first of which was launched in 1962.

Subsequent independent studies by Landon,[1] who analyzed a dual-spin spacecraft with a rigid rotor, and Iorillo,[2] who pioneered the theory showing stability with a nonrigid rotor, suggests that Liapunov stability of the inertial orientation of the spin axis or bearing axis of such a two-body system can be assured by spinning one body about the bearing axis and prescribing a sufficiently small nominal inertial angular velocity for the other body, providing that a damper is located in the "despun" body. Iorillo's paper indicates that if energy dissipation in the rapidly rotating body (the rotor) is known to be in a certain sense small, compared to that in the stationary or slowly rotating body, and if bearings are frictionless, this spin axis stability does not depend upon the presence of a motor or active control system, and it is not contingent upon the satisfaction of any inertia distribution constraints such as those required for simple spinning vehicles.[3]

Reference 4 contains the first published formal proof of dual-spin stability criteria. The proof is restricted to a mathematical model consisting of a rigid platform with an attached rigid, symmetric, frictionless rotor and a damped, linear oscillator. Both rotor axis and oscillator axis parallel a principal axis of the nominal system through its mass center. Extension of formal proof to idealized dual-spin vehicles with linear oscillators on both rotor and despun platform is provided by Mingori.[5]

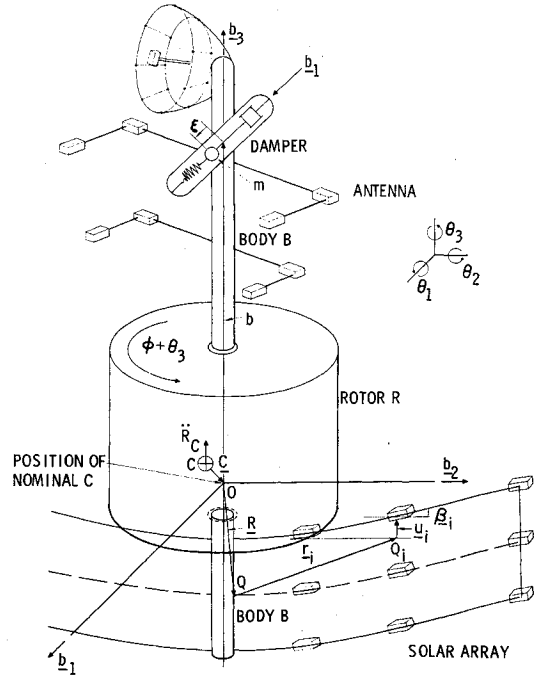

Fig. 1 System schematic and nomenclature.

A great deal of difficult engineering development lies between the enunciation of idealized stability criteria and the launching of satellites. The response to the dual-spin attitude stabilized concept has, nonetheless, been of such magnitude as to alter substantially the field of spacecraft attitude stabilization. A national symposium[6] on attitude stabilization and control of dual-spin spacecraft provided stimulus for industrial and governmental development of this new attitude stabilization concept.

Implementation of the dual-spin attitude stabilization concept requires the introduction of a motor drive between the two primary bodies, with a single-axis active control system required to maintain attitude control of the platform about the bearing axis, compensating for bearing friction. Energy dissipation due to structural damping and any fluid motion within the rotor must be anticipated and compensated for by the passive damper in the platform or, if the bearing axis of the platform is not a principal axis, by the motor and control system. Some provision must be made for the occasional reorientation in inertial space of the system angular momentum vector (e.g., with attitude control jets).

The next generation of dual-spin space vehicles differs from those developed thus far in two apparently incompatible respects; a) allowable pointing errors are an order of magnitude lower, and b) natural frequencies of vibration of flexible antennas and solar panels on the platform are an order of magnitude lower. The present study has been motivated by the need to assess the influence of large, flexible appendages on dual-spin vehicle dynamics and control, in order to establish the feasibility of proposed mission/configuration combinations.

It should be noted explicitly that in this study all flexible appendages are attached to a rigid portion on the despin side of the bearing. The equations are general, but the results are for a model with the rigid portion very small. The vehicle comprises a dual-spin spacecraft which has a nonspinning portion called stator or platform (includes the appendages and a nutation damper), and a large rotor, which may have affixed solar cells and may contain control systems including fuel. This class of vehicle, including damping on both the spinning and nonspinning section, is featured in spacecraft of the Hughes Aircraft Company, known as Gyrostat spacecraft. Since the damper is designed with sufficient margin to offset any damping in the rotor, the equations and simulation referred to in this paper are simplified by assuming no damping on the rotor side of the bearing. Therefore the results, in a broad sense, are also meaningful to spacecraft stabilized by a large momentum wheel.

The equations of vibration for flexible appendages on the spinning rotor have a different structure than those employed here, and different analytical techniques are required. The appropriate generalizations are described briefly in Ref. 7 and developed extensively in Ref. 8. The equations of Refs. 7 and 9 provide the basis for the present system studies, which are documented in greater detail in Ref. 9.

Equations of Motion

Figure 1 is a schematic representation of a hypothetical communications satellite which is typical of the class of vehicles under investigation. It is actually a tri-spin vehicle, since the antenna system is intended to point toward the Earth while the solar panel array remains oriented to the sun. For present purposes both the antenna array and the solar panels are assumed to be nominally nonrotating in inertial space (ignoring the actual rotation of the antenna of the synchronous altitude communications satellite, because

of the length of the twenty-four hour period of rotation). Figure 1 portrays a discrete parameter model of the vehicle, including a rigid symmetric rotor R; a rigid body B pictured as a shaft piercing the rotor; a linear oscillator comprised of a mass m, a spring k, and a dashpot d; and flexible antennas and solar panels represented as collections of elastically interconnected rigid sub-bodies. In practice these sub-bodies are often further idealized as particles.

One confronts a variety of options in the formulation of equations of motion, even after the indicated mathematical model has been selected, Ref. 7 and 8. Although the antennas and solar panels are extremely flexible structures (the solar cells are mounted to a membrane unfurled in space), the quiescence of the space environment justifies in many applications the tentative assumption that deformations of these structures (as represented by $\mathbf{u}^i$ and $\boldsymbol{\beta}^i$ for sub-body $i, i = 1, \ldots n$) are small. Since attention is presently focused on applications for which the body B is nominally inertially at rest, the rotor spin rate relative to the platform $\dot{\varphi}$ is nominally a constant Ω, and the nutation damper displacement ξ is nominally zero, one may define a 1-2-3 set of inertial attitude angles θ_1, θ_2, θ_3 for B and write dynamic equations for the vehicle, linearizing the variables comprising the column matrix

$$x = [\varphi\theta_1\theta_2\theta_3\xi u_1{}^1u_2{}^1u_3{}^1\beta_1{}^1\beta_2{}^1\beta_3{}^1u_1{}^2 \ldots \beta_3{}^n]^T \qquad (1)$$

where $u_\alpha{}^i$ and $\beta_\alpha{}^i$ are defined by $\mathbf{u}^i = u_\alpha{}^i\mathbf{b}_\alpha$ and $\beta^i = \beta_\alpha{}^i\mathbf{b}_\alpha$. Actually φ and $\dot{\varphi}$ are not small, but since φ is cyclic and $\dot{\varphi}$ always appears as a coefficient of a small variable, one can in linearization replace $\dot{\varphi}$ by the constant, Ω, and treat $\ddot{\varphi}$ as small. Unit vectors $\mathbf{b}_1$, $\mathbf{b}_2$, $\mathbf{b}_3$ are a dextral orthogonal set fixed in the rigid platform B.

One may anticipate (and confirm from the derivations[7–9]) that the complete system of equations of motion in the matrix x of small variables will have the structure

$$A\ddot{x} + D\dot{x} + G\dot{x} + Kx = L \qquad (2)$$

where A, D, and K are symmetric constant matrices, and G is a skew-symmetric constant matrix. Matrices D and G owe their presence to the nutation damper and structural damping, and rotor, respectively. In order for the mathematical model illustrated to provide satisfactory simulation of the vehicle, n must be very large. The large dimension of x in Eq. (1) precludes the practical direct solution of Eq. (2); there must first be a transformation to a coordinate matrix which can reasonably be truncated to reduce the number of scalar unknowns. (In practice one might begin with as many as one thousand variables in x, and yet seek to reduce the dimension of the problem so as to retain thirty or fewer variables.)

It should be noted that in the absence of rotor and nutation damper and structural damping, Eq. (2) has the simpler form

$$A\ddot{x} + Kx = L \qquad (3)$$

and one can find a coordinate transformation

$$x = \Phi y \qquad (4)$$

which immediately provides uncoupled second-order equations from Eq. (3). Here the columns of Φ are the eigenvectors of the differential operator in Eq. (3) and, since they are real, the new variables y are real. This is the classical normal modal coordinate approach of structural dynamics.[10] The simplicity of this method suggests that it should be applied to space vehicle dynamics and control problems whenever applicable,[11–13] but this classical approach simply does not apply to Eq. (2), which is appropriate for a dual-spin vehicle with flexible appendages and a nutation damper on a despun platform.

The simplicity of the classical normal modal coordinate approach can be preserved if one abandons the quest for a coordinate transformation which completely uncouples the transformed Eq. (2), and seeks instead to transform only the coordinate matrix

$$q = [u_1{}^1u_2{}^1u_3{}^1\beta_1{}^1\beta_2{}^1\beta_3{}^1u_1{}^2 \ldots \beta_3{}^n] \qquad (5)$$

This uncouples only a subset of the scalar equations implied by Eq. (2). This approach[7–9,14] employs a combination of the discrete scalar coordinates ($\varphi, \theta_1, \theta_2, \theta_3$, and ξ) of rotor, platform, and damper with the distributed or modal coordinates of deformation of the flexible appendages defined by $q = \Phi\eta$ with η truncated. This has been called the hybrid coordinate approach to dynamic analysis, and it is particularly useful for structures which include rotors, dampers, or articulated elements capable of large relative motions.

The objective of the present paper is primarily to describe the results of simulations of immediate practical interest, and secondarily to illustrate for the first time the utility of the hybrid coordinate approach. The derivations of the detailed equations[7–9] are not repeated here.

Equations (34–37) of Ref. 7 are appropriate for a dual-spin system with symmetric rotor, linear oscillator along $\mathbf{b}_1$, and one flexible appendage, so these equations are recorded for application to the system of Fig. 1. (Note that the array of antennas and solar panels in Fig. 1 may be treated as a single appendage on B, or as several appendages, each with equations of motion such as Eq. (7) following. The former approach was used for the results presented herein.) The damper simulation assumes that the damper is attached to the rigid body B, although in practice it is usually attached to the flexible appendage.

$$T = I\ddot{\theta} + \mathcal{J}\ddot{\varphi}E^3 - \mathcal{J}\Omega\tilde{E}^3\dot{\theta} + mb\ddot{\xi}E^2 + m\xi\tilde{E}^1F/\mathfrak{M} + (\tilde{R}\Sigma_{EO}{}^T + \Sigma_{EO}{}^T\tilde{r} + \Sigma_{OE}{}^T)M\Phi\ddot{\eta} - \tilde{F}\Sigma_{EO}{}^TM\Phi\eta/\mathfrak{M} \qquad (6)$$

$$\ddot{\eta} + 2\delta\sigma\dot{\eta} + \sigma^2\eta = -\Phi^TM(\Sigma_{OE} - \tilde{r}\Sigma_{EO} - \Sigma_{EO}\tilde{R})\ddot{\theta} - \Phi^TM\Sigma_{EO}(F - mE^1\ddot{\xi})/\mathfrak{M} + \Phi^T\lambda \qquad (7)$$

$$\tau = \mathcal{J}(\ddot{\varphi} + E^{3T}\ddot{\theta}) \qquad (8)$$

$$m(1 - m/\mathfrak{M})\ddot{\xi} + d\dot{\xi} + k\xi + mbE^{2T}\ddot{\theta} + mE^{1T}F/\mathfrak{M} - mE^{1T}\Sigma_{EO}{}^TM\Phi\ddot{\eta}/\mathfrak{M} = 0 \qquad (9)$$

(In comparing Eq. (6–9) with Eqs. (34–37) of Ref. 7, note that minor misprints in Eq. (35) and (37) have been corrected.) Equation (6) may be identified as providing the three scalar rotational equations of motion for the total vehicle, while Eq. (7–9) provide equations of motion for the appendage, rotor and damper, respectively. The transformation from discrete coordinates q to modal coordinates η of the appendage was chosen so as to uncouple the homogeneous equations of vibration of the appendage [Eq. (7)]. Because the antecedent of Eq. (7) without damping with the variable q has the structure of Eq. (3), this uncoupling can be accomplished directly for the second order equations.

Despin Control System

Equations (6–9) must be augmented by a control law for the control torque τ before the dynamic description is complete. For preliminary studies, a simple proportional control can be assumed, yielding

$$\tau = K_T\theta_3 + C_T\dot{\theta}_3 = K_TE^{3T}\theta + C_TE^{3T}\dot{\theta} \qquad (10)$$

For more realistic simulations, a sampled-data control system illustrated by the block diagram of Fig. 2 is adopted with a shaping network transfer function given by

$$\tau/\epsilon = \{K_c[S^2/\omega_z{}^2 + (2\delta_zS/\omega_z) + 1]\}/\{S[S^2/\omega_p{}^2 + (2\delta_pS/\omega_p) + 1]\} \qquad (11)$$

where tne error ϵ is the difference in command value and observed value of θ_3. Then the torque τ applied to the rotor due to a pointing error ϵ of the platform is available as the

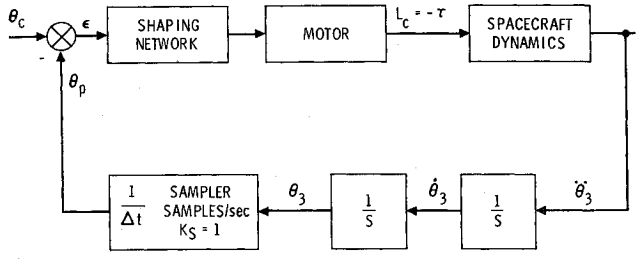

Fig. 2 Spacecraft despin control system.

solution of the differential equation

$$\frac{1}{\omega_p^2}\dddot{\tau} + \frac{2\delta_p\ddot{\tau}}{\omega_p} + \dot{\tau} = +K_c\left(\frac{1}{\omega_z^2}\ddot{\epsilon} + \frac{2\delta_z}{\omega_z}\dot{\epsilon} + \epsilon\right) \quad (12)$$

For the intended application, the command value of θ_3 is generally zero. If attitude errors are sensed continuously, one may substitute for ϵ the difference in command value $\theta_c = 0$ and observed value, θ_3

$$\epsilon = \theta_c - \theta_p = 0 - \theta_3 \quad (13)$$

into Eq. (12) to obtain a third-order differential equation in τ and θ_3.

Continuous sampling is assumed for linearization for the stability investigations based on eigenvalue analyses reported here. Most response simulations have been run with θ_p in Eq. (13) given by

$$\theta_p(t) = \theta_3(t_n) \qquad t_n \leq t < t_{n+1} \quad (14)$$

so $\theta_p(t)$ is held at the value observed for θ_3 during the sampling interval $\Delta t = t_{n+1} - t_n$. For realistic Gyrostat vehicle despin control systems, the sampling interval is the period of rotor rotation (since sensors are rotor-mounted). For values of Δt in near 1 sec the simulation results were essentially equivalent for continuous sensing and sampled data control systems for the configuration investigated.

Stability Determination by Eigenvalue Analysis

First priority goes to the resolution of the following question. If the despin control system is designed on the basis of the assumption that the platform is rigid, will the incorporation of appendage flexibility into the mathematical model result in instability? In mathematical terms, design of the indicated third-order despin control system reduces to selecting numerical values of the gain K_c, the frequencies ω_z and ω_p, and the damping ratios δ_z and δ_p of the lead-lag shaping network. These values are normally selected for preliminary design on the basis of linearized equations such as Eqs. (12, 6, 8, and 9), without any appendage deformations (so $\eta = 0$ in these equations). These equations (with $F = 0$ and external torque $T = 0$) admit a null solution, and the control system is so designed that a solution commencing in the neighborhood of nullity does not diverge. With the accommodation of appendage flexibility, the coordinates η enter the Eqs. (6, 8, and 9), and a new matrix Eq. (7) is included, but still there exists a null solution. Now the question is whether or not for these new equations one still obtains stability for the control system selected in preliminary design.

Although the active control system in a Gyrostat satellite is a single-axis control system, cross-axis coupling is introduced by any realistic representation of the modal response of a flexible appendage as complex as the antenna of Fig. 1. The emphasis in this study has been therefore on the coupled system of linearized Eqs. (6–9) and Eq. (12) reduced to second order, rather than on those portions of these equations corresponding to rotation about the bearing axis. The most efficient approach to the stability analysis of these equations was deemed to be a direct eigenvalue analysis, using computational procedures documented in Ref. 9.

When the external forces and torques [T in Eq. (6) and λ in Eq. (7)] are zero, the stable torque-free dual-spin satellite may be expected to approach asymptotically a state of coincidence of angular momentum vector and "spin axis" or bearing axis assuming perfect rotor balance. The matrix θ in Eqs. (6–9) is comprised of coordinates θ_1, θ_2, θ_3 which establish the platform orientation with respect to an inertially fixed vector basis with the 3-axis paralleling the angular momentum vector prior to perturbation. Subsequent to an arbitrarily small perturbation, the angular momentum vector no longer has the same inertial orientation, and if the spin axis or bearing axis approaches coincidence with this axis after perturbation it will be converging on some arbitrarily small but nonzero value of θ. In other words, one cannot expect a formal indication of asymptotic stability for the null solution of Eqs. (6–9, 12, and 13); at most Liapunov stability can be obtained. This is a consequence of the fact that in terms of the coordinates employed here the damping of this system is not "complete." This subtle distinction and its consequences in stability analysis are examined in detail in Ref. 15; the practical significance here is in the interpretation of the zero eigenvalues which always result from the stability analysis of Eqs. (6–9, 12, and 13). Two zero eigenvalues must be expected because these equations admit (for a perturbed angular momentum) the indicated solution with nonzero constant values of θ_1 and θ_2. Two more zero eigenvalues appear because φ (the rotor angle) is a cyclic coordinate, and one more results from the nature of the control law; Eq. (12) admits a constant solution for torque, τ. Although formally the presence of a zero root of multiplicity five would indicate instability of the linear equation null solution unless the nullity of the corresponding matrix were also five, this conclusion has been suppressed here because interest is limited to Liapunov stability in the variables θ_1, θ_2, θ_3, $\dot{\varphi}$, ξ, η.

Disregarding the indicated zero eigenvalues, one can assess stability and the time constants associated with individual eigenvectors by examining the real part of the eigenvalues of the system. The objective is the convergence of the perturbed solution to a vehicle motion for which the platform

Table 1 System parameters

Parameter	Baseline value (lower, upper limits)
Vehicle	
$\mathfrak{M}$, slugs	53.7(const)
I_{11}, slug-ft^2	1800(1775, 1800)
I_{22}, slug-ft^2	1800(1800, 1825)
I_{33}, slug-ft^2	760(760, 1120)
I_{ij}, $i \neq j$	0(−100, 0)
Appendage	
mass (slugs)	26.9(const)
n (number of sub-bodies)	26(const)
modes of deformation	3(const)
σ_1, Hz	2.0(0.2, 2.5)
σ_2, Hz	2.0(0.2, 2.5)
σ_3, Hz	2.1(0.2, 4.0)
δ_1	0.01 (0, 0.05)
Control system	
K_c	1.5(const)
ω_p, rad/sec	2.5 (1.13, 19.6)
δ_p	0.35 (const)
ω_z, rad/sec	0.14 (0.14, 1.39)
δ_z	1.06 (const)
Nutation damper	
m, slugs	0.1(0.085, 0.2)
frequency, $(k/m)^{1/2}$, rad/sec	1.26 (0.9, 42.)
damping ratio	0.1(0, 0.3)
distance b, ft	13.5(0, 13.5)
Rotor	
$\mathfrak{s}$, slug-ft^2	360(360, 720)
Ω, rad/sec	2π(3.4, 102)

is at rest and the rotor spins about the bearing axis. When this objective is met the system is called stable. In a formal sense this is a special form of Liapunov stability in the noncyclic coordinates of the system, but it is not quite asymptotic stability in these coordinates. The desired stability is reflected in the presence of negative real parts for all but the five zero eigenvalues.

Because of the large number of parameters required to define the system of Fig. 1 and Eqs. (6–9 and 12), the computational procedure involved the selection of a standard or "baseline" configuration, with eigenvalues to be determined for parameter combinations over a spectrum of values including the baseline values. Table 1 lists the system parameters, their baseline values, and the range of variations considered. Of course, not every point in the indicated subspace of the parameter space was considered, but as many as one hundred separate sets of eigenvalues were determined in this region.

In terms of Fig. 1 the baseline configuration has an antenna but no solar panels. The mode shapes Φ^1, Φ^2, and Φ^3 for the baseline modes of the appendage may be characterized as the two transverse bending and torsion modes, respectively, although these terms merely indicate the dominant feature of mode shapes of realistic complexity. The appendage includes everything in the despun section except a small mass on the despun side of the bearing. Deviations from the baseline case include consideration of a vehicle with two solar panels which as cantilevered structures have natural frequencies of approximately 0.3 Hz. Each panel is about 6 × 21 ft and total panel system mass is 4.7 slugs. The few cases investigated indicate no instabilities.

The parameter selection rationale was guided by two objectives; a) establish the influence of appendage flexibility on stability for the baseline configuration, and b) determine whether or not instability could result from even the most injudicious design of a Gyrostat vehicle in the general class of the baseline vehicle.

The first objective led quickly to the conclusion that, for the baseline configuration, the appendage flexibility had a negligible influence on stability. Appendage flexibility for the slightly modified baseline case with the dynamically unbalanced platform again had negligible influence on the system stability. Structural flexibility had a negligible effect on the lead frequency (frequency with numerator of the transfer function) of the despin control system at which θ_3 went unstable (about 0.15 of coning‡ frequency). It was found also that the lag frequency (denominator) of the third-order system could be varied over a wide range with no unstable regions.

Similarly, the effect of structural flexibility on the best damper design for maximizing nutation decay rates was found to be negligible for the baseline configuration.

In pursuit of the objective (*b*), every attempt was made to find a flexible appendage which would destabilize an otherwise stable Gyrostat satellite. Cases were run with all system input frequencies coincident; three appendage natural frequencies, the damper frequency, the proportional despin control system frequency and the vehicle coning frequency. There were no eigenvalues with positive real parts indicative of instability, and the imaginary parts of the eigenvalues indicated a separation of the system natural frequencies. Matrix coefficients were systematically altered to try to achieve some form of resonance, but invariably the system frequencies separated and stability was indicated. Even after numerous runs, instability was never indicated for a vehicle with a "nutation damper," a despin control system without excessive lead frequency, and flexible appendages with minimal damping (as low as 0.25% of critical damping).

‡ The terms "coning frequency," "nutation frequency," and "free precession frequency," are used by various authors to characterize the frequency of rotation of the angular velocity vector in the despun platform or, equivalently, the frequency of rotation of the bearing axis in a conical locus in inertial space.

The divergence of the frequencies, including coning frequency, will be demonstrated analytically from Eqs. (6–9) for a special case in order to establish the conceptual validity of the computer results.

Consider a dual-spin system comprised of a rigid axisymmetric rotor attached to a massless platform with an appendage consisting of a particle of mass μ suspended on a massless elastic cantilever projecting along the extension of the rotor spin axis. Therefore $r = [0\ 0\ r_3]$. For this nominally axisymmetric system, the inertias I_1 and I_2 are identical, and are designated by I. The transformation matrix Φ is simply the identity matrix E, and the inertia matrix for the particle of mass μ is simply μE. The modal coordinate matrix η is $[u_1 u_2 u_3]^T$, where u_i is the particle translation relative to the platform in the ith direction.

The following assumptions were made to facilitate solution of the equations: 1) $T = \tau = 0$, so $\ddot{\varphi} = \ddot{\theta}_3 = 0$ and Eq. (8) and the third equation of Eq. (6) are dropped; 2) $R = 0$ (the base of the cantilever is at the undeformed system center of mass); 3) cantilever stiffnesses along 1 and 2 axes are equal, being represented by spring constant κ, and stiffness along the 3 axis is much greater, so $u_3 \ll u_1$ and u_2. Accordingly, the matrix $\eta = [u_1 u_2 u_3]^T$ is truncated to $\bar{\eta} = [u_1 u_2]^T$. The matrix σ^2 is truncated to $\bar{\sigma}^2 = \sigma_0^2 E$, where E is the 2 by 2 identity matrix and $\sigma_0^2 = \kappa/\mu$; 4) $\delta \equiv 0$ (no structural damping); and 5) $\xi \equiv 0$ and $m = 0$ (the damper is removed), so Eq. (9) is dropped.

From Eqs. (6) and (7) one may now obtain the scalar equations of motion

$$I\ddot{\theta}_1 + \mathcal{I}\Omega\theta_2 - \mu r_3 \ddot{u}_2 = 0 \tag{15}$$

$$I\ddot{\theta}_2 - \mathcal{I}\Omega\theta_1 + \mu r_3 \ddot{u}_1 = 0 \tag{16}$$

$$r_3\ddot{\theta}_2 + \ddot{u}_1 + \sigma_0^2 u_1 = 0 \tag{17}$$

$$-r_3\ddot{\theta}_1 + \ddot{u}_2 + \sigma_0^2 u_2 = 0 \tag{18}$$

Combining these equations into complex form by defining

$$\theta = \theta_1 + i\theta_2 \text{ and } u = u_1 + iu_2 \tag{19}$$

taking the LaPlace transforms of the two resulting equations and finding the characteristic equation, one has after simplification and cancelling the zero root

$$(I - \mu r_3^2)s^3 - i\mathcal{I}\Omega s^2 + I\sigma_0^2 s - i\mathcal{I}\Omega\sigma_0^2 = 0 \tag{20}$$

Because there is no damping, one expects all imaginary roots. Also note that Eq. (20) will be all real with the substitution $s = iw$. Now substitute

$$p = \mathcal{I}\Omega/(I\sigma_0),\ j = I/(I - \mu r_3^2),\ V = v/\sigma_0 \tag{21}$$

to obtain

$$V^3 - pjV^2 - jV + pj = 0 \tag{22}$$

It may be shown[9] that the roots of V are all real (and therefore those of s are all imaginary). The formulae for the roots to a cubic, which is not simply factorable, are so complex that a meaningful exact analytic solution for understanding the phenomena is not attainable. Therefore a graphical solution to Eq. (22) was obtained. The value of μr_3 was chosen to match the transverse inertia of the flexible portion of the complex structure of the baseline vehicle.

Table 2 presents the three roots V_1, V_2, V_3 of Eq. (22). These correspond, respectively, to normalized appendage vibration frequencies in directions 1 and 2 and normalized coning frequency. Note that if the appendage were attached to a fixed base, the values of V_1 and V_2 would be unity. Table 2 also indicates the results of a digital computer eigenvalue analysis of the complex model of the baseline dual-spin vehicle. These frequencies are also normalized by $\sigma_0 = 12.57$ rad/sec.; to permit comparison with the simple model.

The structural frequencies of the simple model are less than 23% higher than those of the complex case. The

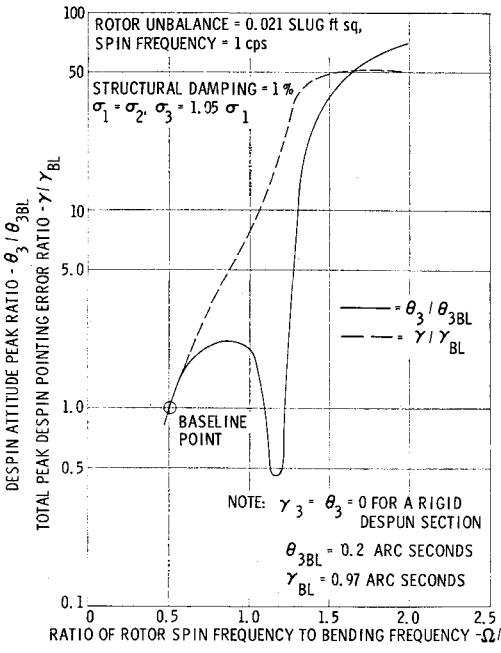

Fig. 3 Effect of rotor spin frequency on peak despin attitude and peak despin pointing error.

ratios of the frequencies of the lateral axes for each case are the same, however. This coupled with the close correlation with coning frequencies, indicates the simplified model is not too bad for verifying the shift in structural frequencies due to gyroscopic stabilization.

Eigenvalue studies indicate a definite change in coning rate, $\dot{\psi}$, when the fixed base frequencies were equal to the rigid $\dot{\psi} = g\Omega/I$. For $p = 1$ the roots of Eq. (22) are $|V| =$ 3.6, 1.25, 0.66. The corresponding reduced frequencies from eigenvalues for the complex system are 2.0, 1.26, 0.76. This corroborates the change in nutation and structural frequency when the structure on the platform is tuned to the rigid body nutation frequency.

In cases where the momentum ratio p is less than one-tenth of the moment of inertia ratio q one can get a rough order of magnitude of the effect on structural frequencies of placing a structure on the platform of a Gyrostat vehicle. Since it is seen that for the baseline case, structural flexibility has a very small effect on coning frequency, one knows that one of the roots of Eq. (20) must be close to $i\dot{\psi} = ig\Omega/I$ or $V = p$ in Eq. (22).

The solution for the other two roots is

$$V = -(p/2)(1-j) \pm \tfrac{1}{2}\{p^2(1-j^2) - 4[p^2(1-j) - j]\}^{1/2} \quad (23)$$

Now for $p \leq 0.1j$ the roots of V are approximately

$$V \simeq -(p/2)(j-1) \pm (j)^{1/2} \simeq \pm[I/(I - mr_3^2)]^{1/2} \quad (24)$$

Therefore, since here V is the structural frequency nondimensionalized by its fixed base frequency σ one can see that the

Table 2 Comparison of normalized natural frequencies of simple and complex models

	Simple [Eq. (22) roots]	Complex [Eqs. (6) and (7) eigenvalues]
V_1 (Vibration in 1 direction)	1.841	1.501
V_2 (Vibration in 2 direction)	1.637	1.333
V_3 (Coning)	0.1003	0.1003
Ratio V_1/V_2	1.13	1.13

Table 3 Gyroscopic effects on structural dynamics

	Damping ratios			Frequencies (cps)		
Mode	Fixed base	$\theta_{ps} = 0$	$\theta_{ps} = 0.07$ rad	Fixed base	$\theta_{ps} = 0$	$\theta_{ps} = 0.07$ rad
1	0.01	0.015	0.015	2.0	3.01	3.07
2	0.01	0.013	0.013	2.0	2.67	2.67
3	0.01	0.096	0.046	2.1	19.42	9.27

frequency of a structure can be expected to go up approximately by the square root of the ratio of the system lateral moment of inertia to the lateral moment of inertia without the flexible portion. In our case $V \approx (3)^{1/2}$ which approximates the more exact values of Table 2.

Eigenvalues also indicated that the structural damping and frequencies in torsion were affected by the tilt of the principal axis of the platform, θ_{ps} (Table 3). This table indicates that one cannot assume fixed base structural frequencies in a Gyrostat system.

Simulation Studies

Equations of motion (6–9, 12, and 14), modified to permit as many as four appendages and a variety of control laws, have been programed§ for digital computer analysis at the Hughes Aircraft Company Space Systems Division. Each appendage can be modeled by up to thirty masses (i.e., $n = 30$), and as many as six modal coordinates per appendage can be retained after truncation (i.e., $N = 6$). Thus for a dual-spin vehicle with rotor, damper, and four appendages on the despun section, as many as twenty-nine coordinates plus those of the control system may be included.

The equations are programed both for numerical integration and (with linearized control law options) for eigenvalue analysis for stability determination. These two programs have produced completely consistent results. Programs are written for the GE 635 computer. The objectives of this simulation were twofold; a) to provide corroboration of the results of eigenvalue studies, b) to permit the accommodation of a sampled data control system, rotor unbalance, and angular momentum control with pulse jets, and c) to assess effects of flexibility on loads and pointing errors.

Objective a) was eventually realized with complete satisfaction. Incorporation of a sampled-data control system proved to have no substantial influence on any aspects of vehicle behavior which related to appendage flexibility. The most significant influence of appendage flexibility was found in the dynamic responses to rotor unbalance and control jet pulsing.

Equations (6) and (8) presuppose a statically and dynamically balanced rigid symmetric rotor, so the bearing axis is the axis of symmetry of the rotor. This idealization is of course physically unrealizable. Current state of the rapidly developing technology of balancing large spinning bodies indicates that an effective balancing uncertainty of eight in. ounces should be assumed for each plane of balance. For these simulations, dynamic unbalance due to an 8 in.-ounce unbalance was assumed to produce an unbalance of 0.021 slug-ft.[2]

If the bearing axis is a principal axis of the platform, so there is no product-of-inertia coupling between the pointing angle θ_3 and the angles θ_1 and θ_2, there is no error in θ_3 introduced by rotor unbalance. Appendage flexibility does provide this coupling, however, so it must be expected that θ_3 (as well as θ_1 and θ_2) will be influenced by rotor unbalance for dual-spin vehicles with flexible appendages. Figs. 3 and 4 illustrate these influences.

The solid line in Fig. 3 illustrates the influence on platform pointing angle θ_3 of the ratio of spin frequency to structural

§ The expert programing of M. Hunt of Hughes Aircraft Company is gratefully acknowledged.

fundamental frequency σ_1. The ordinate is normalized by the baseline value of 0.2 arcsec, and is on a logarithmic scale.

The dashed line in Fig. 3 is of greater practical interest than the solid line, because its ordinate is not the maximum pointing error of θ_3 of the platform but the actual pointing error γ of the flexible antenna, which performs torsional oscillations about the platform bearing axis. The baseline normalization for this case is 0.97 arcsecs, so the antenna pointing error approaches one minute in this figure.

Figure 4 portrays the influence of the ratio of spin frequency Ω to structural bending frequency σ_1 on the coning angle, as represented by θ_2. The ordinate is again normalized by the value of θ_2 (2.8 arcsec) for the baseline configuration, which in this case is essentially the same as the value for θ_2 when the antenna is presumed rigid, 3.0 arcsec.

Some unexpected effects of rotor unbalance may be observed (Figs. 3 and 4). The deflections of the structure in both bending and torsion increase with a power of approximately 3.5 of the inverse of frequency σ_1, even away from resonance points (a power of near 2 was expected). This would appear to be because the lateral deflections are expected to be predominantly outward causing higher centrifugal force which in turn increases the lateral deflections. The lateral deflections cross-couple into the torsional mode increasing torsional deflections. These in turn increase the stator despin pointing error θ_3 hence they magnify deflections γ.

The exception to flexibility increasing coning is in the vicinity where the fixed base frequency equals the spin rate ($\Omega/\sigma_1 = 1$). Here the coning angle decreases. Evidently the phasing is such that the coning angle of the spinning portion is decreased even though deflections do increase through this regime (Fig. 3). (Note that the rate of increase is somewhat decreased near $\Omega/\sigma_1 = 1$ in that figure.) The regime where θ_2 is less than the rigid case is between 0.5 and 0.75 of the bending frequencies in the Gyrostat system where the spin rate is in resonance. Thus structure and coning motion can be out of phase at least part of the time. The values of the abscissa where the bending frequencies in the system coincide with the spin rates are 1.32 and 1.56. Here we see the typical effects of resonance in both pointing (Fig. 3) and coning (Fig. 4). Plots of the peak lateral forces and moments at the base of the platform indicate typical resonance curves. They are essentially flat to about $\Omega/\sigma_1 = 1.2$ and then rise to peak in the neighborhood of $\Omega/\sigma_1 = 1.5$.

The influence of flexible appendages on the dynamic response to impulsive torques applied by attitude control jets was briefly documented in Ref. 7, which was written when the study reported here was in progress. During 20 sec of pulsing at 1-sec intervals on the baseline configuration there is accumulated a 15-arcsec error in θ_3 and a total of 41 arcsec of error in the antenna pointing angle, γ. This result is based on the assumption of 5-lb control jets located 4 ft from the mass center and applying a square wave pulse of duration 0.111 sec. All of this error can be attributed to the antenna flexibility, since for a dynamically balanced platform there is no coupling to provide error in θ_3 due to

Table 4 Effect of platform product of inertia on pointing error for the baseline configuration

	Due to unbalance		Due to control pulsing	
	Peak pointing error γ arcsecs	Coning angle θ_2 arcsecs	γ arcsecs	θ_2 arcsecs
Baseline, $\theta_{ps} = 0$	0.97	2.8	41	160
Baseline, $\theta_{ps} = 0.07$ rad	1.47	2.8	166	160

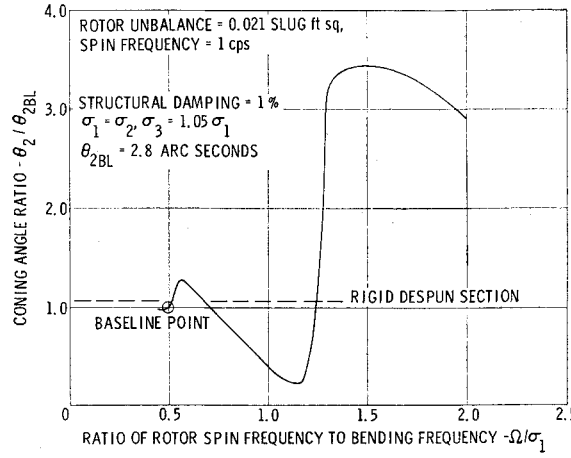

Fig. 4 Effect of rotor spin frequency and structural frequencies on coning angle.

transverse torques. (It should be remembered that for a synchronous altitude satellite, a 40 arcsec pointing error corresponds to about 6.7 naut miles in southern United States and some satellite designs seek better accuracy than is permitted by this error caused by flexibility alone.)

In addition to the preliminary data offered in Ref. 7, Fig. 5 can now be added, in order to illustrate the variation in maximum pointing error γ (previously reported as 38 arcsec) with changes in certain frequency ratios. The curve indicates (perhaps surprisingly) the desirability of having similar jet pulsing frequency and fundamental vibration frequency, and the corresponding undesirability of having the platform torsional mode frequency σ_3 so close to the transverse bending frequency $\sigma_1 = \sigma_2$.

The former is primarily due to the shift in structural frequency when a structure is in the despun portion of a Gyrostat spacecraft. This should be accounted for in interpretation of these results as in the previous results.

The effects of a tilt in principal axis of the platform of 0.07 radians was spot checked. The shapes of the curves in Eqs. (4–6) are similar but the magnitude of pointing error is increased substantially according to Table 4. Most of the change is due to rigid body motion.

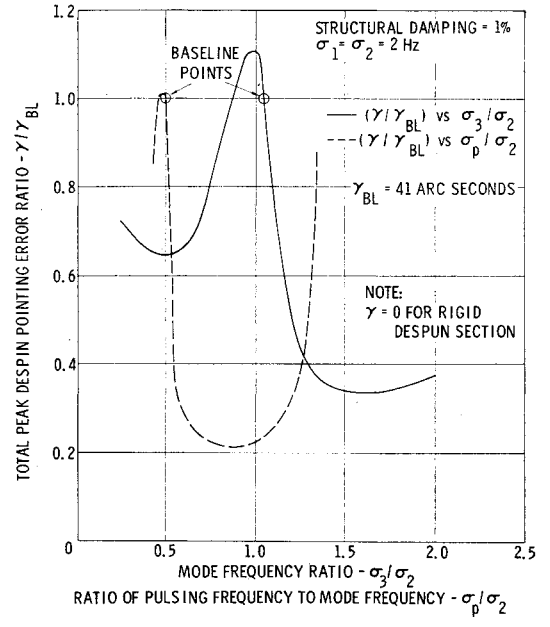

Fig. 5 Coupling effects of structural frequencies and control system pulsing on total despin pointing error.

Conclusions

For a class of dual-spin vehicles with a flexible platform constituting roughly half of the vehicle mass, and having structural vibration frequencies in the neighborhood of 2 Hz, the following conclusions may be drawn from this study:

1) Stability is not influenced by the flexible platform, as long as the appendages have at least a minimal amount of structural damping. (Preliminary investigation of a Gyrostat vehicle with relatively small flexible solar panels with natural frequencies as low as 0.3 Hz also failed to reveal any instabilities due to flexibility.)

2) The relations among control jet pulsing frequencies, structural vibration frequencies, coning frequencies, and (for the unbalanced rotor) spin frequencies have a definite influence on pointing accuracy, although for no system examined did the attitude error attributable to antenna flexibility exceed one minute of arc except for the case with the principal axis of the platform tilted.

3) The despin control system and nutation damper can be designed independently of structural flexibility with reasonable assurance that stability and nutation damping time characteristics will be essentially the same as for the flexible case if there is a reasonable amount of structural damping (>0.5%).

These are very encouraging conclusions, which suggest an unexpected advantage of dual-spin satellites over those having three-axis active control. The latter are known to exhibit instability due to flexibility in some situations,[16] and their performance characteristics seem also to be more severely impaired by flexibility. Primary reasons for this may be found in the substantial resistance to attitude errors provided by the stored angular momentum, and in the presence of the attitude sensors and thrusters on the relatively rigid rotor of the vehicle.

References

[1] Landon, V. D. and Stewart, B., "Nutational Stability of an Axisymmetric Body Containing a Rotor," *Journal of Spacecraft and Rockets*, Vol. 1, No. 6, June 1964, pp. 682–684.

[2] Iorillo, A. J., "Nutational Damping Dynamics of Axisymmetric Rotor Stabilized Satellites," American Society of Mechanical Engineers Winter Meeting, Nov. 1965, Chicago, Ill.

[3] Bracewell, R. N. and Garriott, O. K., "Rotation of Artificial Earth Satellites," *Nature*, Vol. 182, Sept. 1958, pp. 760–762.

[4] Likins, P. W., "Attitude Stability Criteria for Dual-Spin Spacecraft," *Journal of Spacecraft and Rockets*, Vol. 4, No. 4, 1967, pp. 1638–1643.

[5] Mingori, D. L., "Effects of Energy Dissipation on the Attitude Stability of Dual-Spin Satellites," *AIAA Journal*, Vol. 7, No. 1, Jan. 1969, pp. 20–26.

[6] "Proceedings of the Symposium on Attitude Stabilization and Control of Dual-Spin Spacecraft," Air Force Rept. SAMSO-TR-68-191; also Rept. TR-0158 (3307-01)-16, Nov. 1967, Aerospace Corp.

[7] Likins, P. W. and Gale, A. H., "The Analysis of Interactions Between Attitude Control Systems and Flexible Appendages," Paper IAF AD29, Oct. 1968, 19th International Astronautical Congress.

[8] Likins, P. W., "Dynamics and Control of Flexible Space Vehicles," TR 32-1329, Feb. 1969, Jet Propulsion Lab.

[9] Gale, A. H. and Likins, P. W., "A Study of the Dynamics of Spacecraft with Flexible Appendages with Special Attention to a Gyrostat with a Flexible Despun Section," Aerospace Technology Research Rept. SSD 90003R, Jan. 1969, Hughes Aircraft Co.

[10] Hurty, W. C. and Rubinstein, M. F., *Dynamics of Structures*, 2nd ed., Prentice Hall, Englewood Cliffs, N.J., 1964, Chap. 3, p. 135.

[11] Ashley, H., "Observations of the Dynamic Behavior of Large Flexible Bodies in Orbit," *AIAA Journal*, Vol. 5, No. 3, March 1967, pp. 460–469.

[12] Likins, P. W., "Modal Method for Analysis of Free Rotations of Spacecraft," *AIAA Journal*, Vol. 5, No. 7, 1967, pp. 1304–1308.

[13] Gevarter, W. B., "Basic Relations for Control of Flexible Vehicles," AIAA Paper 69-115, New York, Jan. 1969.

[14] Likins, P. W., and Wirsching, P. H., "Use of Synthetic Modes in Hybrid Coordinate Dynamic Analysis," *AIAA Journal*, Vol. 6, No. 10, Oct. 1968, pp. 1867–1872.

[15] Likins, P. W. and Mingori, D. L., "Liapunov Stability Analysis of Freely Spinning Systems," *Proceedings of the 18th International Astronautical Congress*, Belgrade, Yugoslavia, Sept. 1967, pp. 89–102.

[16] Likins, P. W. and Fleischer, G. E., "Results of Flexible Spacecraft Attitude Control Studies Utilizing Hybrid Coordinates," AIAA Paper 70-20, New York, Jan. 1970.